J Therm Anal Calorim (2017) 129:601–607
DOI 10.1007/s10973-017-6151-5

Calorimetric analysis of non-crystalline $TeO_2–V_2O_5–Sb_2O_3$

Determination of crystallization activation energy, Avrami index and stability parameter

Dariush Souri[1] · **Yazdan Shahmoradi**[1]

Received: 14 May 2016 / Accepted: 6 February 2017 / Published online: 18 February 2017

Abstract In the present report, thermal and physical characterization of $40TeO_2–(60 - x)V_2O_5–xSb_2O_3$ glasses, prepared by melt quenching method, has been investigated by differential scanning calorimetry (DSC) and so discussed in the compositional range $0 \leq x \leq 10$ mol%. DSC plots of these ternary glasses have been studied within the temperature range of 150–500 °C at the heating rates $\varphi = 3$, 6, 9, 10 and 13 K min^{-1}. In this work, thermal stability, glass-forming tendency, the temperature corresponding to the onset of crystallization (T_x), the crystallization temperature (T_{Cr}), the glass transition temperature (T_g), the activation energy of crystallization by using Ozawa and Kissinger methods, and the crystallization activation energy using Avrami index (n) have been measured and reported, to determine the relationship between Sb_2O_3 content and the thermal stability in order to interpret the structure of glass. In conclusion, from the obtained data, it was found that characteristic temperatures T_g, T_x and T_{cr} are increasing with increasing the antimony oxide content and also with increasing the heating rate; glass with $x = 10$ has the highest thermal stability and glass-forming tendency and so has very good resistance against thermal attacks; the sample S5 shows a sharp decrease in the crystallization activation energy, which can be resulted by the increase in non-bridging oxygens; the crystallization activation energy calculated from Kissinger's model is more accurate, and the trend of activation energy values is similar in all of Ozawa, Kissinger and Avrami methods; also the obtained values of n show that it fluctuates around $n \approx 1$, which can be attributed to surface or one-dimensional crystal growth of crystals.

Keywords Amorphous materials · Ozawa method · Kissinger method · Avrami index · Crystallization activation energy

Introduction

Transition metal-containing oxide glasses (TMOGs) have received increased interest due to their technological advantages in optical fibers nonlinear optical devices [1–3] and in electrochemical applications [4, 5]. Also, due to the attractive and unique properties of tellurium-based TMOGs such as good electrical conductivity, low melting point, low hygroscopy and appropriate colorimetric properties, they have been the subject of many works. However, the change in the mole percentage of the glass components results in the desirable physical properties of the samples [6–14]. Differential scanning calorimetry (DSC) is a powerful and convenient method to study the thermal behavior of glass at different heating rates. The onset of crystallization (T_x), the crystallization temperature (T_{Cr}), the glass transition temperature (T_g) are obtained from DSC measurement [15–23]; these measurements used to calculate the crystallization activation energy from methods Ozawa, Kissinger and Avrami index [16]. Kinetics of crystallization process can be described by the activation energy for crystallization (ΔE), and the Avrami index (n) reflects the characteristics of nucleation and the growth process [17]. It should be mentioned that the present glasses, $TeO_2–V_2O_5–Sb_2O_3$, have been studied in our previous works, for their optical [24], electrical [25], glass transition [26] and elastic [26] properties. But there is no

---

✉ Dariush Souri
d.souri@gmail.com; d.souri@malayeru.ac.ir

[1] Department of Physics, Faculty of Science, Malayer University, Malayer, Iran

report on the kinetics of crystallization process and Avrami exponent of these glassy systems. So, this work aims at:

1. Investigation of the crystallization temperature and crystallization activation energy in several heating rates.
2. Determination of ΔE by using the different approaches named as Kissinger, Ozawa and Avrami.
3. Study of the compositional dependence of T_{cr} and ΔE.
4. Introducing the strong samples with higher thermal stability, having higher resistance against thermal shocks in applications.

Materials and methods

The bulk non-crystalline samples of the composition $(60 - x)$ V_2O_5–$40TeO_2$–xSb_2O_3 glasses with $0 \leq x \leq 10$ (in mol%) were prepared by well-known melt quenching method; Hereafter, the samples are nominated as S*x*. Reagent grades of starting powders were mixed by grinding the mixture to provide a fine powder; then, the mixture was melted in alumina crucible in an electric furnace under the ordinary atmosphere and so the melt was poured on a steal block to be quenched. Non-crystallinity nature of the powdered samples was confirmed by powder XRD. The details of materials and methods for glass preparation, structural characterization and also calorimetric analysis can be followed in our previous works on the same composition [24–26].

Results

XRD patterns profiles

Powder XRD profiles of S*x* samples confirm that the quenched melts are vitreous, as the patterns can be found in our previous work on these samples [24].

Thermal analysis by DSC

The typical DSC curves of S0 are shown in Fig. 1. The DSC curves show a glass transition correspond to temperature T_g that we usually just take the middle endothermic region. This transition is followed by exothermic peaks corresponding to crystallization temperatures T_{cr}; moreover, the onset temperature of crystallization process is named as T_x. Also, the base line before T_g can certify the glassy feature of the understudied samples. The mentioned characteristic temperatures are listed in Table 1 [20]. It is known that the area under the crystallization peak is proportional to the heating rate [21, 22]; but as could be seen in Fig. 1, nevertheless of repeated measurements, it is not obeyed at the heating rate of 10 K min^{-1} for S0.

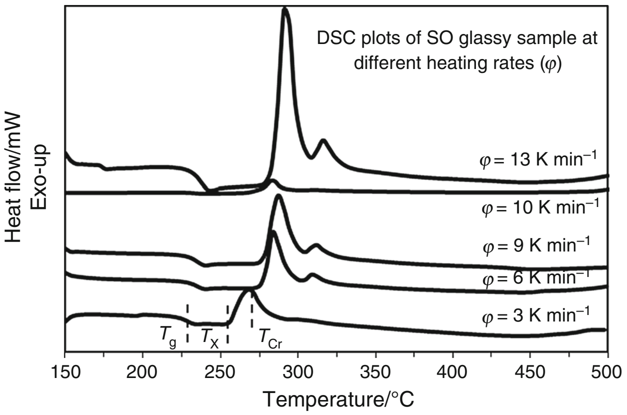

Fig. 1 DSC outputs of S0 at several heating rates (φ)

Determination of crystallization activation energy using Ozawa and Kissinger approaches

Kissinger [27] and Ozawa [28] methods are well-known methods for the study of calorimetric feature of glasses. Ozawa formula is as follows [28]:

$$d\ln(\varphi)/d(1/T_x) = -\Delta E/R_g, \tag{1}$$

which can be used to calculate the crystallization activation energy (ΔE); where T_x is the onset temperature of crystallization process and R_g is the universal gas constant [16]. However, in Ozawa method, the slope of the plot of $\ln(\varphi)$ versus $1/T_x$ results in determination of $(\Delta E/R_g)$ and so obtaining the ΔE value. Such plot is shown in Fig. 2 for the understudied glasses, and the results for all the compositions are scheduled in Table 1.

Also, Fig. 3 shows the plots $\ln T_{Cr}^2/\varphi - 1/T_{Cr}$ upon Eq. 2 (Kissinger formula), which give the $(\Delta E/R_g)$ values. The results of ΔE for all the compositions are shown in Table 1.

$$\ln\left(T_{cr}^2/\varphi\right) = \left(\Delta E/R_g T_{cr}\right) + \text{const} \tag{2}$$

The activation energy for crystallization was in the range 56.459–141.404 kJ mol^{-1} and 71.710–119.713 kJ mol^{-1} in Kissinger and Ozawa methods, respectively.

The graph of ΔE versus Sb_2O_3 content is shown in Fig. 4, which indicates the similar trend and near values of ΔE in both Kissinger and Ozawa approaches.

Calculation of the Avrami index and the crystallization activation energy by using modified Kissinger formula

The Kissinger formula is often used for crystallization and also glass transition data analysis [17, 21–23]. The

Table 1 Thermal and physical data of S*x* glasses: glass transition temperature (T_g), the onset temperature of crystallization (T_x), melting point (T_m), crystallization temperature (T_{Cr}), thermal stability ($\Delta T = T_{cr} - T_g$), the crystallization activation energy in Kissinger method ($\Delta E_{Kissinger}$), in Ozawa method (ΔE_{Ozawa}) and modified Kissinger (ΔE_{Avrami}), Avrami index (n), the volume fraction of crystals (α)

Sample	φ/K min^{-1}	T_g/°C [26]	T_{cr}/°C	T_m/°C [26]	T_x/°C	$\Delta T = T_{cr} - T_g$/°CΔ	$\Delta E_{Kissinger}$/kJ mol^{-1}	ΔE_{Ozawa}/kJ mol^{-1}	n	V_m/cm^3 mol^{-1} [26]	α	ΔE_{Avrami} kJ mol^{-1}
S0	3	227.70	267.15	680	249.261	39.450	141.404	119.713	0.830	46.623	0.32021	115.872
	6	232.68	283.20		268.755	50.520					0.18236	
	9	233.78	286.80		272.302	53.020					0.238897	
	10	234.80	287.50		275.036	52.700					0.158648	
	13	235.96	290.642		275.131	54.682					0.078409	
S5	3	253.10	326.84	720	291.88	73.74	56.459	71.710	1.432	47.235	0.999968	85.769
	6	257.70	352.00		321.075	94.300					0.966959	
	9	261.10	366.575		334.375	105.470					0.910022	
	10	261.60	380.058		345.044	118.458					0.913974	
	12	264.20	382.675		348.25	118.475					0.660886	
S8	3	269.60	397.60	740	371.825	128.000	93.707	117.177	1.0486	47.230	0.419468	98.828
	6	274.10	421.70		392.375	147.600					0.424692	
	9	276.40	438.80		410.375	162.400					0.227949	
	10	277.50	444.10		402.557	166.600					0.228702	
	12	281.60	449.60		413.875	168.00					0.09448	
S10	3	273.91	423.107	750	401.801	149.197	93.283	90.489	1.1357	46.898	0.593824	98.000
	6	278.52	466.931		405.658	188.411					0.250937	
	9	284.61	470.671		409.351	186.068					0.190964	
	10	284.67	472.557		410.049	187.887					0.154844	
	13	284.75	474.127		446.646	189.377					0.174605	

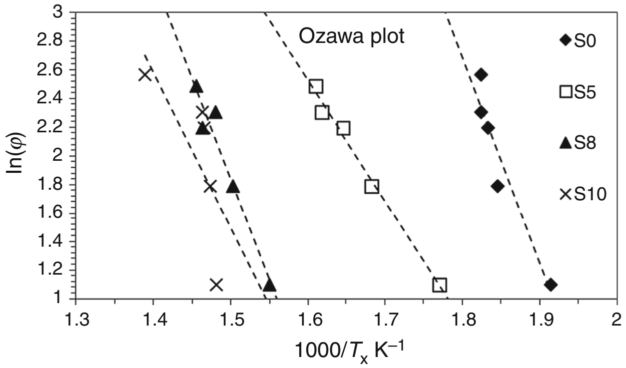

Fig. 2 Ozawa plots for S*x* glasses upon Eq. 1

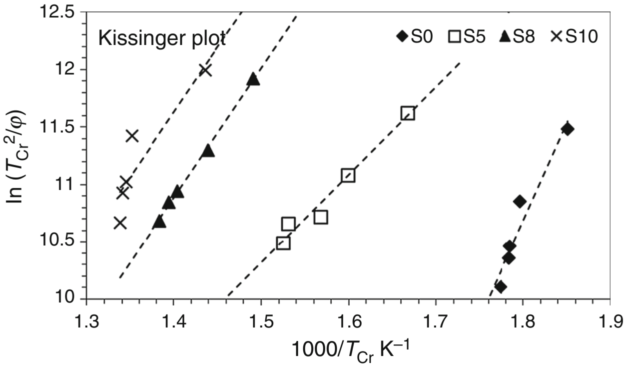

Fig. 3 Kissinger plots (upon Eq. 2) for S*x* glasses

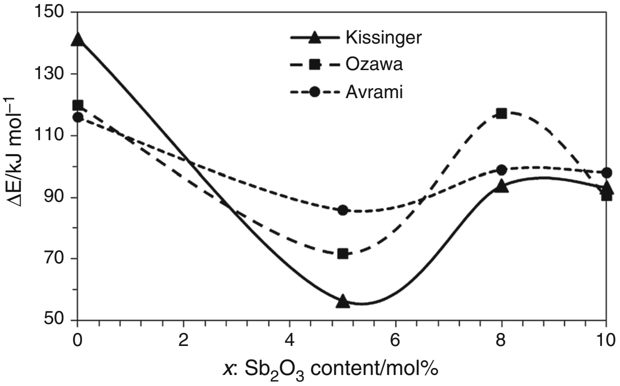

Fig. 4 Crystallization activation energy (Δ*E*) as a function of Sb_2O_3 content in Ozawa and Kissinger and modified Kissinger (Avrami) methods

modified form of the Kissinger equations is as follows [17, 21–23]:

$$\ln\left(\varphi^{n}/T_{cr}^{2}\right) = -(m \cdot \Delta E)/\left(R_g\, T_{cr}\right) + \text{const} \tag{3}$$

where as mentioned before, φ is the heating rate, Δ*E* is the activation energy, *n* and m are the Avrami exponent (index) and the dimensionality of the crystal growth, correspondingly. Generally the parameters *n* and *m* are heating rate dependent.

From the curves of ln $(\varphi^n/T_{cr}^2) - 1/T_{cr,}$ one can obtain Δ*E*, *n* and *m* [17]. Moreover, value of n can be obtained from Eq. 4 as below [17, 21–23]:

$$n = -\mathrm{d}\{\log[-\ln(1-\alpha)]\}/\mathrm{d}\log\varphi \tag{4}$$

In this equation, α is the volume fraction of formed crystals during the crystallization process. So, α can be obtained using a software for partial area analysis. Furthermore, at a typical selected temperature α is introduced by:

$$\alpha = A/A_o \tag{5}$$

As depicted in Fig. 5, A_o is the total area under the crystallization curve between the temperature T_x (as the onset temperature of crystallization) and temperature T_2 (as the crystallization termination temperature) and *A* is the area between T_x and selected *T*.

The obtained data of α are listed in Table 1. Figure 6 shows typically the plot of log [−ln(1 − α)] versus logφ for S8 sample. As is clear from Eq. 4, the value of *n* can be obtained from the slop of log [−ln(1 − α)] versus logφ plots. The obtained values were in the range of $0.83 \le n \le 1.43$. These values are close to $n = 1$, which is the feature (can be attributed to) for one-dimensional or surface crystallization. Selected temperatures are 280, 385, 396 and 426.6 K for S0, S5, S8 and S10, respectively. However, according to the obtained *n* values, the crystallization activation energy (Δ*E*) can be obtained from modified Kissinger equation (Eq. 3); it should be noted that the amount of m is considered equivalent 1 [17]. Figure 7 shows the Plots of $\ln(\varphi^n/T_{cr}^2)$ versus $1000/T_{cr}$.

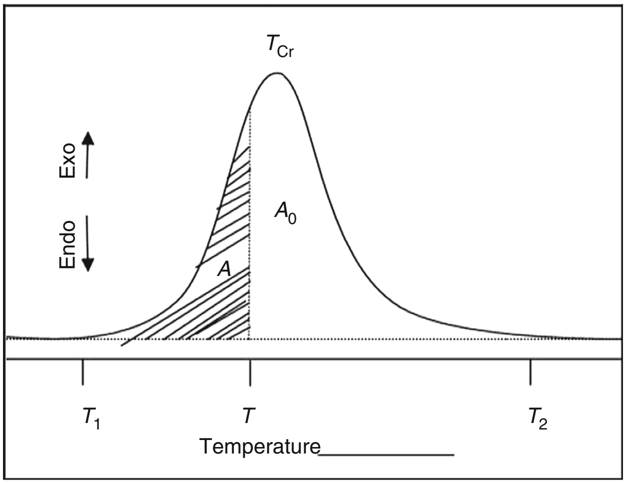

Fig. 5 Graphical representation of a typical crystallization peak in DSC curves, to be used for α volume fraction of formed crystals (α) by partial area analysis

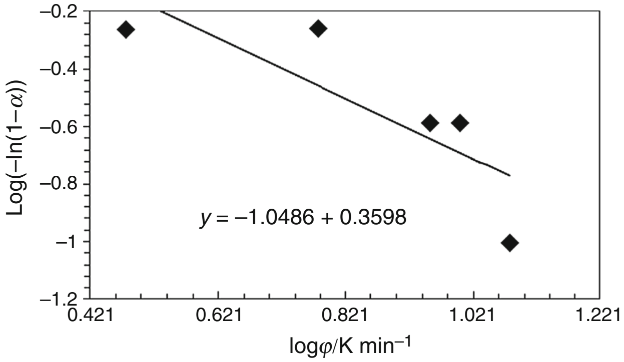

Fig. 6 Plot of log [−ln(1 − α)] versus log φ for S8 sample; n is the slope of the plot as 1.0486. The related data of other samples are presented in Table 1

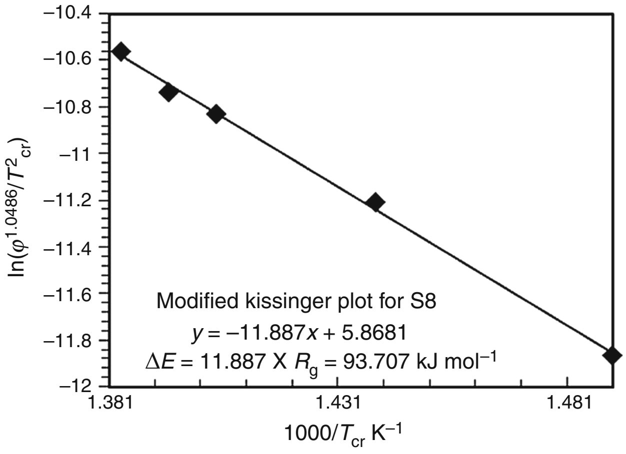

Fig. 7 Plot of ln (φ1.0486/T_{cr}^2) versus 1000/T_{cr} for S8 upon Eq. 3

According to the obtained values of Avrami index and using Eq. 3, the activation energy of Sx samples was calculated and the results for all the compositions are listed in Table 1.

Figure 4 shows the Avrami activation energy changes with Sb_2O_3, and the sample S5 shows a sharp decrease in the crystallization activation energy, which can attributed to the increase in non-bridging oxygens (NBOs). It should be noted that in the sample preparation, glasses with higher amounts of antimony oxide were not formed and colorimetric analysis was done merely by four.

Thermal stability

The glass thermal stability is often defined as $\Delta T = T_{cr} - T_g$ [29]. The thermal stability of the glass is a very important parameter of fundamental and technological aspects and is a scale of the degree of disorder in glass structure. In the process of making optical fibers, materials affected temperatures higher than the T_g; If the glass is a weak and has low thermal stability, crystallization occurs during the heating process; therefore, the formed crystalline phases can scatter input signal and signal transport cannot perform with good efficiency [29, 30]. According to the data T_g, T_{cr} and ΔT in Table 1, Fig. 8 shows the increasing trend of thermal stability versus Sb_2O_3 content; therefore, glass with $x = 10$ has the highest thermal stability and glass-forming tendency and so has very good resistance against thermal attacks, which is an excellent criteria for technological advantages [26].

Discussion

In this study, the linear correlation coefficient of plots (R^2) was closer to 1 in Kissinger method, in comparison with Ozawa and modified Kissinger approaches. Therefore, Kissinger method is more suitable for the study of these samples. Despite the difference in the amount of activation energy in all three models, the results are nearly same. (see Fig. 4; Table 1). The difference in the amount of ΔE may be due to differences in determining the exact amount of T_x and T_{cr}. In general, the crystallization activation energy calculated from Kissinger's model is more accurate and the trend of activation energy values is similar in all of Ozawa, Kissinger and Avrami methods. All three methods are physically equivalent and have a good validation for the crystallization process. The sample S5 shows a sharp decrease in the crystallization activation energy, which can be attributed to the increase in non-bridging oxygens (NBOs); this means an increase in glass fragility. To certify the above statements

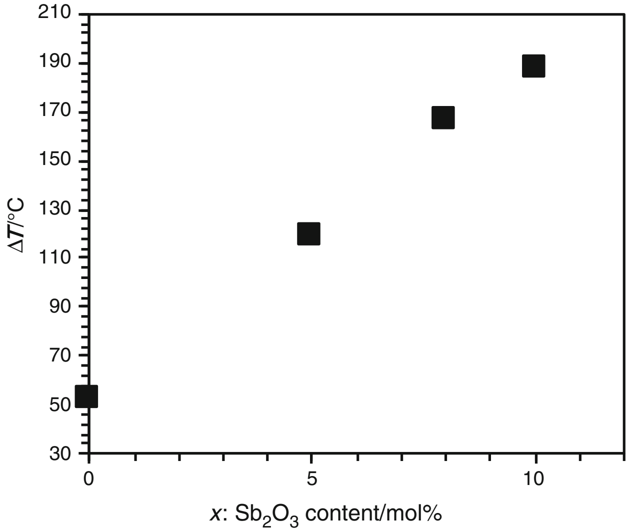

Fig. 8 Dependence of thermal stability to Sb_2O_3 content at a typical heating rate of 10 K min^{-1}

and in comparison between the results of S0 and S5, one can observe that although the crystallization temperature increases, the activation energy decreased and S5 has the minimum activation energy among the other samples; it seems that one can attribute this result to the molar volume of the present glasses (taken from ref. [26]); as listed in Table 1, S5 has maximum molar volume, denoting its more opening and loose structure, probably due to dangling bonds and NBOs affecting the thermal properties. Also, according to the data from Table 1, samples S8 and especially S10 have the highest thermal stability and crystallization activation energy; thus, S10 has the highest stability and so lowest fragility.

Conclusions

From the investigation of glass transition temperature, the temperature corresponding to the onset of crystallization (T_x), melting temperature (T_m) crystallization temperature (T_{Cr}) at the different heating rates (φ), thermal stability ($\Delta T = T_{cr} - T_g$), the crystallization activation energy from Kissinger method ($\Delta E_{Kissinger}$), the crystallization activation energy from Ozawa method (ΔE_{Ozawa}), Avrami index (n) and the crystallization activation energy from modified Kissinger (Avrami) method (ΔE_{Avrami}) of $(60 - x)V_2O_5$–$40TeO_2$–xSb_2O_3 Ternary glasses, one can present the following conclusions:

1. The samples are amorphous in nature.
2. Glass with $x = 10$ has the highest thermal stability and glass-forming tendency, the lowest fragility and so has very good resistance against thermal attacks; also, the glass S8 has relatively good stability.
3. The sample S5 shows a sharp decrease in the crystallization activation energy, which can be a result of the increase in non-bridging oxygens.
4. The crystallization activation energy calculated from Kissinger's model is more accurate, and the trend of activation energy values is similar in all of Ozawa, Kissinger and modified Kissinger (Avrami) methods.
5. According to the results, the amount of the Avrami index was $0.830 \leq n \leq 1.432$ and activation energy obtained in this way is $85.69\ \text{kJ mol}^{-1} \leq \Delta E_{Avrami} \leq 115.872\ \text{kJ mol}^{-1}$, respectively.
6. The n values show this value is close to $n = 1$ which is characteristic for one-dimensional or surface crystallization growth.

Compliance with ethical standards

Conflict of interest The authors declare that they have no conflict of interest.

References

1. Golis EP, Reben M, Wasylak J, Filipecki J. Investigations of tellurite glasses for optoelectronics devices. Opt Appl. 2008;XXXVIII:163–9.
2. Murugan GS, Ohishi Y. TeO_2–BaO–SrO–Nb_2O_5 glasses: a new glass system for waveguide devices applications. J Non-Cryst Solids. 2004;341:86–92.
3. Wang Y, Dai S, Chen F, Xu T, Nie Q. Physical properties and optical band gap of new tellurite glasses within TeO_2–Nb_2O_5–Bi_2O_3 system. Mater Chem Phys. 2009;113:407–11.
4. Pal M, Hirota K, Tsujigami Y, Sakata H. Structural and electrical properties of MoO_3–TeO_2 glasses. J Phys D Appl Phys. 2001;34:459–64.
5. Lebrun N, Levy M, Souquet JL. Electronic conductivity in glasses of the TeO_2–V_2O_5–MoO_3 system. Solid State Ion. 1990;40:718–22.
6. Souri D. Fragility, DSC and elastic moduli studies on tellurite–vanadate glasses containing molybdenum. Measurment. 2011;44:1904–8.
7. Angell CA. Relaxation in liquids, polymers and plastic crystals—strong/fragile patterns and problems. J Non-Cryst Solids. 1991;131–133:13–31.
8. Souri D. Glass transition and fragility of telluro-vanadate glasses containing antimony oxide. J Mater Sci. 2012;47:625–31.
9. Souri D, Mohammadi M, Zaliani H. Effect of antimony on the optical and physical properties of Sb–V_2O_5–TeO_2 glasses. Electron Mater Lett. 2014;10:1103–8.
10. El-Mallawany R. Specific heat capacity of semiconducting glasses: Binary vanadium tellurite. Phys Status Solidi A. 2000;177:439–44.
11. El-Mallawany R, Abousehly A, Yousef E. Elastic moduli of tricomponent tellurite glasses TeO_2–V_2O_5–Ag_2O. J Mater Sci Lett. 2000;19:409–11.
12. Souri D. Study of the heating rate effect on the glass transition properties of (60 − x) V_2O_5–xSb_2O_3–$40TeO_2$ oxide glasses using differential scanning calorimetry (DSC). Measurement. 2011;44:2049–53.
13. Souri D. Investigation of glass transition temperature in $(60 - x)$ V_2O_5–$40TeO_2 - x$NiO glasses at different heating rates. J Mater Sci. 2011;32:6998–7003.
14. Souri D, Tahan ZE, Salehizadeh SA. DC electrical conductivity of Ag_2O–TeO_2–V_2O_5 glassy systems. Indian J Phys. 2016;90:407–15.
15. Wunderlich B. Thermal analysis. New York: Academic Press; 1990. p. 1370–401.
16. Souri D. Crystallization kinetic of Sb–V_2O_5–TeO_2 glasses investigated by DSC and their elastic moduli and Poisson's ratio. Phys B. 2015;456:185–90.
17. Grujic S, Blagojevic N, Tosic M, Zivanovic V, Nikolic J. Crystallization kinetics of $K_2O{\cdot}TiO_2{\cdot}3GeO_2$ glass studied by DTA. Sci Sinter. 2008;40:333–8.
18. Vijayan C, Soundararajan N, Chandramohan R, Ramaswamy S, Gnanadurai P. The effect of heating rate on the phase transition and crystallization kinetics of $Ag_2Se_{0.2}Te_{0.8}$ alloy. J Therm Anal Calorim. 2015;119:91–7.
19. Svoboda R, Malek J. Crystallization mechanisms occurring in the Se–Te glassy system. J Therm Anal Calorim. 2015;119:155–66.
20. Lesz S, Dercz G. Study on crystallization phenomenon and thermal stability of binary Ni–Nb amorphous alloy. J Therm Anal Calorim. 2016;126:19–26.
21. Aly KA, Othman AA, Abousehly AM. Effect of Te additions on the glass transition and crystallization kinetics of $(Sb_{15}As_{30}Se_{55})_{100-x}Te_x$ amorphous solids. J Alloys Compd. 2009;467:417–23.

22. Aly KA, Saddeek YB, Dahshan A. Effect of WO_3 on the glass transition and crystallization kinetics of borotellurite glasses. Philos Mag. 2010;90:4429–41.
23. Aly KA, Hassaan MY, Saddeek YB. Thermal features and physical properties of sulfur modified barium vanadate glasses. Phase Transit. 2013;86:477–89.
24. Souri D, Shomalian K. Band gap determination by absorption spectrum fitting method (ASF) and structural properties of different compositions of $(60 - x)$ V_2O_5–$40TeO_2$–xSb_2O_3 glasses. J Non-Cryst Solids. 2009;355:1597–601.
25. Souri D. Small polaron hopping conduction in tellurium based glasses containing vanadium and antimony. J Non-Cryst Solids. 2010;356:2181–4.
26. Souri D. DSC and elastic moduli studies on tellurite-vanadate glasses containing antimony oxide. Eur Phys J B. 2011;84:47–51.
27. Kissinger HE. Variation of peak temperature with heating rate in differential thermal analysis. J Res Nat Bur Stand. 1956;57:217–21.
28. Ozawa T. Kinetics of non-isothermal crystallization. Polymer. 1971;12:150–8.
29. Kumar MP, Sankarapa T, Awasthi AM. Thermal and electrical properties of some single and mixed transition metal ions doped tellurite glasses. Phys B. 2008;403:4088–95.
30. Zoubos H, Koutsokeras LE, Anagnostopoulos DF, Lidorikis E, Kalogirou SA, Wildes AR, Kelires PC, Patsalas P. Broadband optical absorption of amorphous carbon/Ag nanocomposite films and its potential for solar harvesting applications. Sol Energy Mater Sol Cells. 2013;117:350–6.